Origin of the large piezoelectric activity in $(1 - x)\text{Ba}(\text{Zr}_{0.2}\text{Ti}_{0.8})\text{O}_3$-$x(\text{Ba}_{0.7}\text{Ca}_{0.3})\text{TiO}_3$ ceramics

Matias Acosta,[1,2,*] Nasser Khakpash,[3] Takumi Someya,[2] Nikola Novak,[1] Wook Jo,[4] Hajime Nagata,[2]
George A. Rossetti, Jr.,[1,3] and Jürgen Rödel[1]

[1]*Institute of Materials Science, Technische Universität Darmstadt, 64287 Darmstadt, Germany*
[2]*Faculty of Science and Technology, Tokyo University of Science, 278-8510 Noda, Japan*
[3]*Institute of Materials Science, University of Connecticut, Storrs, Connecticut 06269, USA*
[4]*School of Materials Science and Engineering, Ulsan National Institute of Science and Technology, 689-798 Ulsan, Republic of Korea*

The diffusionless pseudobinary phase diagram, monodomain properties, and free energy of $(1 - x)\text{Ba}(\text{Zr}_{0.2}\text{Ti}_{0.8})\text{O}_3$-$x(\text{Ba}_{0.7}\text{Ca}_{0.3})\text{TiO}_3$ are computed for comparison with experimental results. Specifically, the variation of the spontaneous polarization, anisotropy energy, and free energy with respect to temperature, composition, and polarization direction are discussed relative to the results of resonant piezoelectric measurements performed over a wide compositional range as a function of temperature. The phase angle, relative permittivity, piezoelectric and coupling coefficients, and elastic compliances were used to investigate relations between the computed and measured pseudobinary phase diagrams and the measured piezoelectric and elastic properties. It was found that d_{33} values along the orthorhombic to tetragonal phase boundary are ∼30% higher than those both along the rhombohedral to orthorhombic phase boundary and in the region where phases converge. It is shown that the reduction in anisotropy energy in these regions of the phase diagram is by itself insufficient to explain the measured properties. The highest small signal piezoelectric activity is found along the orthorhombic to tetragonal phase boundary due to a combination of reduced anisotropy energy, high remanent/spontaneous polarization, and increased elastic softening. The combined computed and experimental results are used to demonstrate that the interdependent behavior of these properties should be considered in the design of engineered piezoelectric ceramics.

PACS number(s): 77.65.−j

I. INTRODUCTION

Piezoelectric materials are used in a large variety of technological devices such as actuators, transducers, sensors, filters, and switches. Lead zirconate-titanate (PZT) is by far the most widely used material for these applications [1]. In 2003 the European Union proposed to limit the use of hazardous materials in consumer products [2]. Specifically, it was determined that lead in functional ceramics is to be substituted as soon as comparable nontoxic materials are available [2,3]. More than ten years after the original directive and a subsequent update of the "Restriction of the Use of Certain Hazardous Substances in Electrical and Electronic Equipment" [3], there is no single all-encompassing materials solution. However, several breakthroughs have been noted [4]. In particular, new materials based on engineered phase boundaries in potassium sodium niobates are available [5,6]. These materials can be co-sintered with cost-effective nickel electrodes [7], which is not currently achievable for PZT [8]. Tou *et al.* [9] laid the groundwork for hard bismuth-based piezoceramics to be used in ultrasonic cleaners, and Doshida *et al.* [10,11] demonstrated that lead-free piezoceramics have better performance than PZT for high power applications. Recently, a BaTiO_3 (BT)-based solid solution, $(1 - x)\text{Ba}(\text{Zr}_{0.2}\text{Ti}_{0.8})\text{O}_3$-$x(\text{Ba}_{0.7}\text{Ca}_{0.3})\text{TiO}_3$ (BZT-xBCT), has attracted considerable attention due to its promising small and large signal piezoelectric properties [12,13]. Because of its low Curie temperature, however, the BZT-xBCT system is inherently limited to low-temperature applications. Nevertheless, it remains useful

for specific applications where working temperatures do not exceed 90 °C [13,14]. The first prototype products based on this material have already been shown to have adequate performance [15]. Considering the technological importance of BZT-xBCT, it is of interest to elucidate the mechanism behind its exceptional small signal piezoelectric properties.

The origins of the strong piezoelectric response observed in BZT-xBCT materials are still under investigation. In other ferroelectric solid solutions, the role played by monoclinic (M) phase(s) [16,17], disorder in the displacement of cations [18,19], formation of nanodomains [20,21], and two-phase coexistence [22,23] have been invoked to explain enhanced functional properties near phase boundaries. Despite the differing interpretations of the structural state near phase boundaries, it has been argued that a reduction in the crystalline anisotropy of polarization, as recognized in the earliest studies of PZT, is the central phenomenon connected with large piezoelectric activity [24,25]. The underlying interpretation is that along phase boundaries an extreme reduction in the crystalline anisotropy of polarization leads to a degeneration of the energy surface to near spherical symmetry. This automatically results in an instability of the polarization vector against rotation, the formation of miniaturized domains with a large number of symmetry-equivalent orientations [26,27], and to a region in the phase diagram wherein ferroelectric phases differing in symmetry may coexist as metastable states [28]. For BZT-xBCT it was further proposed that the coincidence of triple and tricritical points along the Curie line may result in a reduction of the anisotropy energy that extends along the phase boundary lines separating the lower-temperature ferroelectric phases [12]. The reduced energy barrier for polarization

───────
*acosta@ceramics.tu-darmstadt.de

rotation in the region projected below the tricritical point was in turn associated with exceptional small signal piezoelectric properties [12].

Although the model proposed by Liu and Ren [12] was based on the presence of a tricritical point, the pseudobinary phase diagram of BZT-xBCT has not been definitively established. Recent reports have proposed the existence of rhombohedral (R), tetragonal (T), and orthorhombic (O) phases that converge near the line of Curie temperatures [13,29,30]. This region has thus been termed a "phase convergence region." Nevertheless, recent computations show that two triple points are expected in this region, although these two points may be difficult to access experimentally due to their close proximity [31]. Therefore, the current picture of the pseudobinary phase diagram of BZT-xBCT involves two lines of polymorphic phase boundaries (PPTs) with an interleaving single phase or two-phase coexistence region separating the commonly accepted R and T phases. The nature of the interleaving region remains unresolved and is characterized either as an O single phase [13,14,29,30] or as a coexistence region of R and T phases [32–34]. Regardless of the nature of the structural state in this region, the reduction of the anisotropy energy is thought to play an important role. In early reports on the BZT-xBCT system the local maxima in dielectric and piezoelectric properties observed in this region were attributed to reduced anisotropy energy [12,13]. The pseudobinary phase diagram of BZT-xBCT was recently estimated using a phenomenological approach and a sharp reduction of the anisotropy energy along the PPTs' lines and in the phase convergence region was demonstrated [31]. Therefore, enhancement of dielectric and piezoelectric properties is expected in the vicinity of the convergence region [12,27]. In contrast, recent experimental investigations have shown that the small signal piezoelectric properties are maximized along the O to T phase boundary, and that only local maxima are obtained in the phase convergence region [13,30]. Moreover, the two PPTs also give rise to different small signal piezoelectric activities [13]. Therefore, the complex small signal properties of BZT-xBCT cannot be fully explained by considering only the reduction of the anisotropy energy. Neglecting extrinsic contributions to small signal properties, other physical properties such as elastic response and remanent polarization should be fully investigated across the whole phase diagram to accurately describe the small signal piezoelectric activity. Indeed, it was recently highlighted that the elastic properties are of key importance in determining piezoelectric response of this system [30,35,36].

In this paper, the pseudobinary phase diagram of BZT-xBCT is analyzed by means of a phenomenological theory and experimental results. The variation of the spontaneous polarization, anisotropy energy, and stability of the T, O, and R phases along the PPTs are computed. These results are compared with resonance-antiresonance piezoelectric measurements obtained as a function of temperature over a wide compositional range. By correlating the computational and experimental results, the role of a reduction in anisotropy energy, elastic properties, and spontaneous/remanent polarization in enhancing the functional properties of BZT-xBCT is clarified.

II. MATERIALS AND METHODS

A. Thermodynamic phenomenology

The classical Landau theory is applicable to second-order displacive phase transitions and weak first-order transitions close to second order [37,38]. The Landau polynomial describing the nonequilibrium free-energy density of perovskite-structured ferroelectrics is most commonly expressed in the form given by Devonshire [Eq. (1)] [39,40],

$$G_L = \tfrac{1}{2}\alpha_1\left(P_1^2 + P_2^2 + P_3^2\right) + \tfrac{1}{4}\alpha_{11}\left(P_1^4 + P_2^4 + P_3^4\right)$$
$$+ \tfrac{1}{2}\alpha_{12}\left(P_1^2 P_2^2 + P_1^2 P_3^2 + P_2^2 P_3^2\right) + \cdots. \tag{1}$$

Here P_i are components of the polarization vector and it is to be understood that the dielectric stiffness coefficients $\alpha_{i\ldots}$ are analytical functions of the external variables of temperature, pressure, and/or composition. The equilibrium free energies of the symmetry-allowed proper ferroelectric phases are determined by minimizing the thermodynamic potential [Eq. (1)] with respect to components of polarization.

In reproducing the phase diagrams of ferroelectric solid solutions, it is advantageous to employ an alternative Landau polynomial which explicitly separates the isotropic and anisotropic contributions to the free energy, the latter determining the interferroelectric phase transitions between proper symmetry phases [27,41]. This alternative polynomial can be written as given in Eq. (2),

$$G_L = \tfrac{1}{2}\alpha_1\left(P_1^2 + P_2^2 + P_3^2\right) + \tfrac{1}{4}\big[\beta_1\left(P_1^2 + P_2^2 + P_3^2\right)^2$$
$$+ \beta_2\left(P_1^4 + P_2^4 + P_3^4\right)\big] + \tfrac{1}{6}\big[\gamma_1\left(P_1^2 + P_2^2 + P_3^2\right)^3$$
$$+ \gamma_2\left(P_1^6 + P_2^6 + P_3^6\right) + \gamma_3\left(P_1^2 P_2^2 P_3^2\right)\big] + \cdots. \tag{2}$$

The polynomial in Eq. (2) is equivalent to that in Eq. (1) and the two can be interchanged using a set of linear relations between the expansion coefficients [31]. The isotropic part of the free energy in Eq. (2), ($G_{L\text{iso}}$), formally describes a polarized state with modulus of polarization $P \neq 0$ in which there is no preferential polarization direction [Eq. (3)],

$$G_{L\text{iso}} = \tfrac{1}{2}\alpha_1 P^2 + \tfrac{1}{4}\beta_1 P^4 + \tfrac{1}{6}\gamma_1 P^6 + \cdots. \tag{3}$$

The anisotropic part of the free energy in Eq. (2), ($G_{L\text{aniso}}$), determines the dependence of the free energy on the direction of the polarization vector. The anisotropic part of the free energy is given in Eq. (4):

$$G_{L\text{aniso}} = \tfrac{1}{4}\big[\beta_2\left(P_1^4 + P_2^4 + P_3^4\right)\big]$$
$$+ \tfrac{1}{6}\big[\gamma_2\left(P_1^6 + P_2^6 + P_3^6\right) + \gamma_3\left(P_1^2 P_2^2 P_3^2\right)\big] + \cdots. \tag{4}$$

The proper ferroelectric phases with different symmetries are determined by the anisotropic part of the free energy [Eq. (4)], in which the direction of the polarization vector is treated as an internal thermodynamic variable that relaxes to the equilibrium direction subject to changes in external variables (temperature, pressure, and/or composition). For the T, O, and R proper ferroelectric phases the equilibrium direction of the polar vector is oriented along the [001], [110], and [111] crystallographic directions of the cubic prototype, respectively [42,43]. The stable ferroelectric phase

for a particular choice of external variables has the lowest (most negative or least positive) anisotropy energy with respect to the other phases [31]. Because the phase diagrams for BCT and BZT are known, the coefficients in the free-energy function [Eq. (2)] can be determined and used to estimate the pseudobinary phase diagram along the isopleth $(1-x)\text{Ba}(\text{Zr}_{0.2}\text{Ti}_{0.8})\text{O}_3$-$x(\text{Ba}_{0.7}\text{Ca}_{0.3})\text{TiO}_3$ [31]. The equation of state is determined from Eq. (2) using the minimum principle and gives the corresponding equilibrium properties of interest here, e.g., spontaneous polarization, anisotropy energy, and free energy. These properties were computed from room temperature up to $100\,°\text{C}$ and in the compositional range of interest corresponding to $(1-x)\text{Ba}(\text{Zr}_{0.2}\text{Ti}_{0.8})\text{O}_3 - x(\text{Ba}_{0.7}\text{Ca}_{0.3})\text{TiO}_3$ $(0.32 \leqslant x \leqslant 0.60)$. The resolution of the calculation was selected to be 128×128 points over this range of composition and temperature. Contour plots were constructed by interpolation between the calculated points.

B. Experiments

In order to enable a comparison with the phenomenological computations, a series of ceramics with the compositions $(1-x)\text{Ba}(\text{Zr}_{0.2}\text{Ti}_{0.8})\text{O}_3 - x(\text{Ba}_{0.7}\text{Ca}_{0.3})\text{TiO}_3$ $(0.32 \leqslant x \leqslant 0.60)$ were produced via a mixed oxide route using BaCO_3 (purity 99.8%, Alfa Aesar), TiO_2 (purity 99.6%, Alfa Aesar), CaCO_3 (purity 99.5%, Alfa Aesar), and ZrO_2 (purity 99.5%, Alfa Aesar, Germany). Complete details for the processing conditions can be found elsewhere [13]. Bar-shaped samples of $2 \times 2 \times 5\,\text{mm}^3$ were machined for the measurements. The samples were electroded with silver paste and burnt-in at $400\,°\text{C}$ for 2 h with a heating rate of 2 K/min.

The resonance-antiresonance piezoelectric measurement is a well-established characterization technique from which a set of piezoelectric, dielectric, and elastic properties can be obtained for a specified geometry excited in a given vibration mode [44]. The 33 mode describes the longitudinal response of a bar-shaped sample with respect to polarization direction [44]. Dielectric, electromechanical, and elastic properties, including the phase angle θ, relative permittivity $\varepsilon_{33}^{\text{T}}/\varepsilon_0$, piezoelectric charge coefficient d_{33}, coupling coefficient k_{33}, mechanical quality factor Q_{m}, elastic compliances s_{33}^{E} and s_{33}^{D}, and frequency constant N_{33} can be computed from this measurement. In order to determine these properties, complex impedance measurements were carried out on all samples by the resonance-antiresonance method using an impedance analyzer (Hewlett Packard HP4294A, United States) in the 33 mode. A 500-mV peak to peak sinusoidal wave in the kHz range (corresponding to the resonance-antiresonance of each sample) was utilized as the input voltage. *In situ* temperature-dependent measurements were performed from 25 to $105\,°\text{C}$ in $5\,°\text{C}$ steps. Prior to each measurement the temperature was stabilized within $\pm 0.2\,°\text{C}$ in order to satisfy thermal equilibrium conditions. All samples were poled at room temperature for 10 min with an electric field strength of 4 kV/mm to ensure a poled state [13]. From these measurements electromechanical properties (d_{33}, k_{33}, and Q_{m}), elastic compliances (s_{33}^{E} and s_{33}^{D}), and frequency constant (N_{33}) were obtained according to the IEEE standard on piezoelectricity [44]. The maximum phase angle θ obtained at each isotherm was also recorded. From the recorded measurements, composition-temperature contour plots were constructed with a resolution of 7×15 points within the range of composition and temperature examined. The variation of properties between the measured points was estimated by linear interpolation between them.

III. RESULTS

A. Phenomenological predictions

The pseudobinary phase diagram of BZT-xBCT was reproduced using the form of the low-order Landau polynomial described in the previous section. This approximation has recently been demonstrated to provide a good agreement with experimental results for both BT-based and PbTiO_3-based perovskite solid solutions [31,45]. The dependencies of the coefficients of the Landau polynomial on composition and temperature were formulated to self-consistently reproduce the known phase diagrams of BZT and BCT. Linear interpolation of these coefficients along the isopleth $(1-x)\text{Ba}(\text{Zr}_{0.2}\text{Ti}_{0.8})\text{O}_3$-$x(\text{Ba}_{0.7}\text{Ca}_{0.3})\text{TiO}_3$ resulted in the phase diagram shown in Fig. 1. The close agreement of the phase boundaries with available experimentally determined phase diagrams [13,14,29] strongly indicates that the low-order approximation of the theory provides an adequate representation of the free energies of the different phases within their respective stability regions. The derivatives of these free energies give the property coefficients of the monocrystalline, monodomain state. In polycrystalline ceramics, however, there are a number of extrinsic contributions that lead automatically to quantitative differences between computed and measured polycrystalline-averaged properties. Hence, phenomenological predictions made here are intended to describe the qualitative behavior of the system, but not necessarily to provide a quantitative description of materials properties.
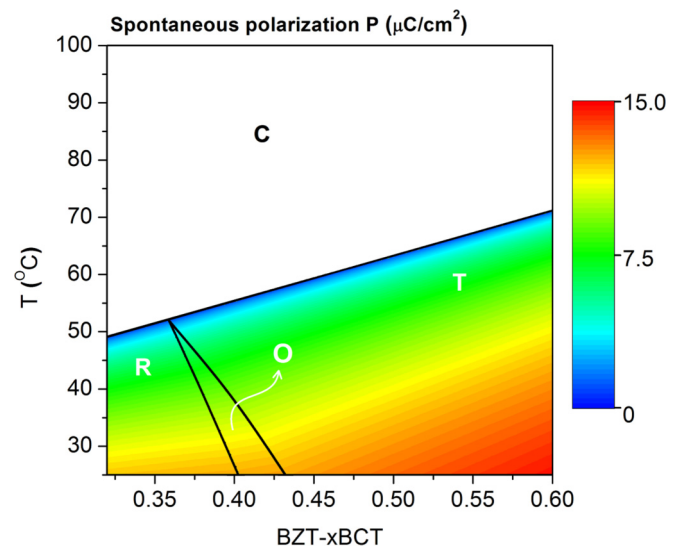

FIG. 1. (Color online) Variation in the spontaneous polarization superimposed on the computed composition-temperature pseudobinary phase diagram of BZT-xBCT. The resolution of the contour plot in the composition-temperature space is 128×128. The variation of polarization between the calculated points was estimated by linear interpolation between them.

The variation in the modulus of the equilibrium polarization (*P*) with composition and temperature is also shown in Fig. 1 and is superimposed on the predicted phase boundary lines of BZT-*x*BCT. Good qualitative agreement is found with recently proposed experimental pseudobinary phase diagrams [13,14,29]. Although the interleaving region between *R* and *T* phases is predicted to be a homogeneous *O* phase, this phase is nearly degenerate with the *R* and *T* phases. Hence, the possibility of two-phase coexistence cannot be excluded, as has been previously proposed [32–34]. The computed monodomain polarization values are found to provide good qualitative agreement with experiments [12,13]. A slight jump in polarization associated with weak first-order transitions was observed at the *R* to *O* and *O* to *T* phase boundaries. The magnitude of these jumps diminishes as the convergence region is approached. The small jumps in polarization at the phase boundaries are a direct consequence of the reduced anisotropy energy in this region of the phase diagram. Furthermore, it should be noted that the polarization values increase substantially on moving away from the phase boundaries and into the *T* phase. These findings are consistent with previous phenomenological analyses which have considered the anisotropy energy of BT [46].

The calculated phase diagram features a stability region of the *O* phase. The stabilization of this phase is most favored in this region due to reduced anisotropy energy. This strong reduction can be more clearly observed by examining the (1̄10) section of the energy surface on passing through the sequence of *R* → *O* → *T* transitions. This sequence of transitions occurs as the temperature is increased at fixed compositions close to interferroelectric phase boundaries. Such a section is shown in Fig. 2, where the free energy is plotted as function of the angle ($0 \leqslant \varphi \leqslant 2\pi$) of the polar vector measured with respect to the [001] direction. This section of the energy surface includes the polar directions of the *T*, *O*, and *R* phases. Three compositions $x = 0.38$, $x = 0.40$, and $x = 0.42$ as a function of temperature were chosen as representative examples. The free-energy curves are normalized with respect to the value of the free energy of the stable phase at each temperature and composition in order to facilitate comparisons at each set of conditions. The *R* phase is the stable phase at low temperatures in compositions with $x = 0.38$ and 0.40, while the *O* phase is stable for $x = 0.42$. As temperature increases, the energy profile corresponding to the *R* phase flattens leading to a stable *O* phase. With further temperature increase the *T* phase emerges while the *O* phase may persist in a small temperature interval as a metastable phase. The emergence of the *T* phase is accompanied by an increase in barrier heights along the free-energy profiles. As depicted in Fig. 2, the energy profiles are relatively flat throughout the entire stability region of the *O* phase, i.e., the *O* phase is nearly degenerate with the *T* and *R* phases in this region of the phase diagram. The appearance of lower symmetry phases such as those experimentally observed [16,19,29,30] is a consequence of this extreme reduction in the free-energy anisotropy. It is illustrated in Fig. 2 that for compositions and temperatures close to phase boundaries, the anisotropic contributions to the free energy shrink to about 1% of the total free energy. This reduction is a feature of both the convergence region ($x \sim 0.38$, $T \sim 45\,^{\circ}$C) as well as PPTs (*R* to *O* $x \sim 0.40$, $T \sim 35\,^{\circ}$C; *O* to *T* $x \sim 0.42$, $T \sim 25\,^{\circ}$C).
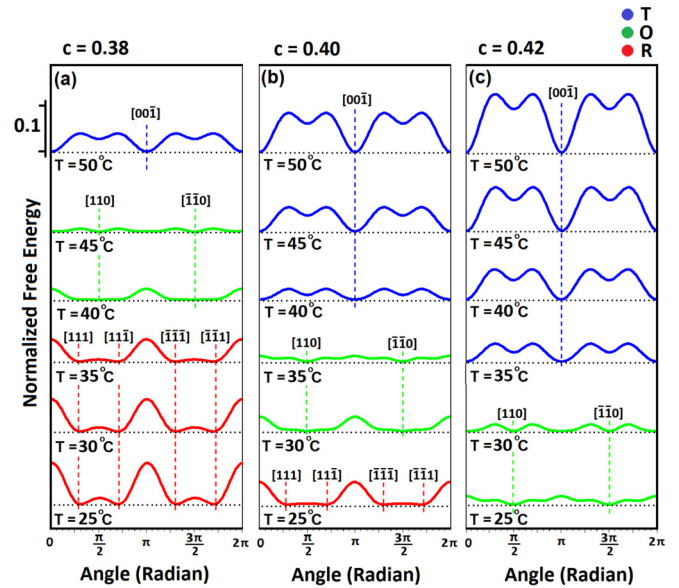

FIG. 2. (Color online) Energy variation with polarization rotation in (1̄10) plane starting from [001] direction as temperature increases from 25 to 50 °C at three compositions (a) 0.38, (b) 0.40, and (c) 0.42. The stability regions of rhombohedral (*R*), orthorhombic (*O*), and tetragonal (*T*) phases are illustrated in red, green, and blue colors, respectively. The free-energy curves are normalized with respect to the value of the free energy of the stable phase at each temperature and composition.

Figure 3 presents the anisotropy energy superimposed on the computed phase diagram of BZT-*x*BCT. The reduction in anisotropy energy can be seen as a tilted "Y"-shaped area adjacent to PPTs and along the Curie line. This region broadens
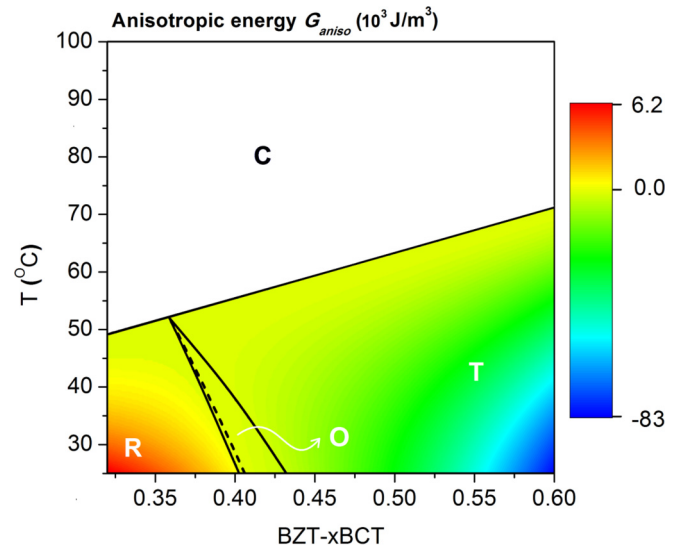

FIG. 3. (Color online) Anisotropy energy superimposed on the computed composition-temperature pseudobinary phase diagram of BZT-*x*BCT. The dashed line indicates vanishing of the free-energy anisotropy. The resolution of the contour plot in the composition-temperature space is 128 × 128. The variation of anisotropy energy between the calculated points was estimated by linear interpolation between them.
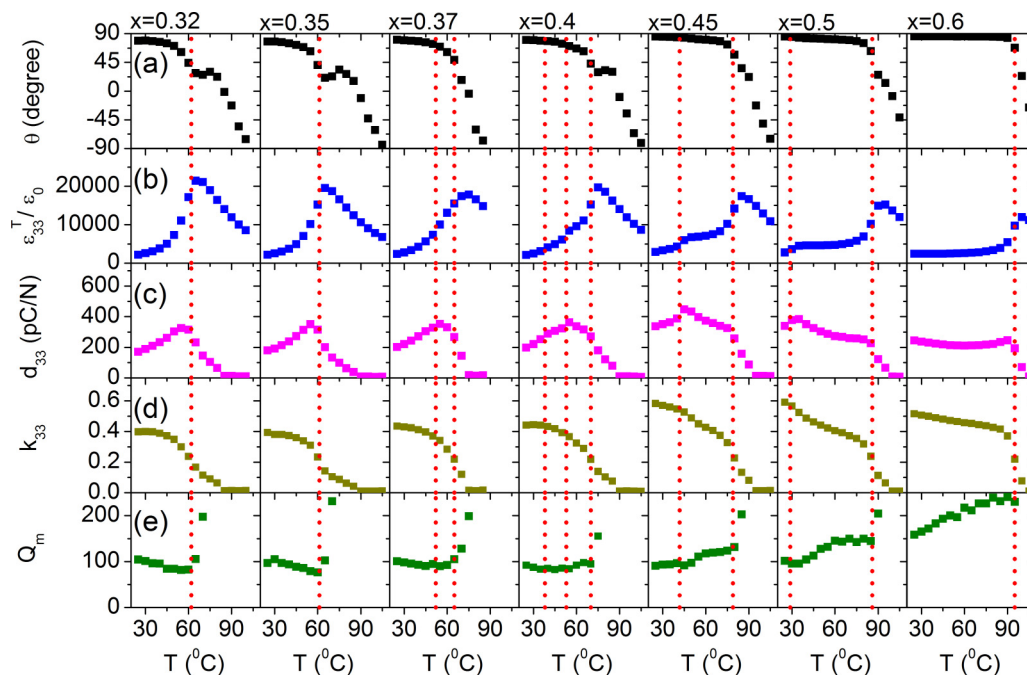
FIG. 4. (Color online) Piezoelectric and dielectric properties as function of temperature for compositions from $x = 0.32$ to 0.6. (a) phase angle θ, (b) relative permittivity $\varepsilon_{33}^T/\varepsilon_0$, (c) small signal d_{33}, (d) coupling factor k_{33}, and (e) mechanical quality factor Q_m obtained from resonance-antiresonance data. Dotted lines indicate phase transitions [13].

substantially at higher temperatures and extends along the Curie line. This result is reflected in the energy profiles of the T phase becoming more anisotropic with increasing temperature at $x = 0.40$ and 0.42 at temperatures above 50 °C (Fig. 2). The dashed line in Fig. 3 indicates the locus of points where anisotropy energy vanishes. It is clearly shown that vanishing of the anisotropy energy occurs in the vicinity of the R to O phase boundary but does not coincide with it.

The reduction of the anisotropy energy near interferroelectric phase boundaries leads to miniaturized domains [47] and to divergence of the transverse dielectric susceptibility [41,42]. The domain structure and electromechanical properties of ferroelectric solid solutions also show a strong dependence on the curvature of these phase boundaries [31]. The strong inclination of the phase boundaries as observed for BZT-xBCT (denominated here as PPTs according to Goldschmidt [48]) is accompanied by a broad area of reduced anisotropy energy. In contrast, in solid solutions with a nearly vertical morphotropic phase boundary [48], the region of reduced anisotropy is very narrow at low temperatures and only broadens substantially at high temperatures near the Curie line. The strongly tilted phase boundaries observed for BZT-xBCT are accompanied by a broad area of the composition-temperature plane in which the anisotropy energy is dramatically reduced. This leads to the degeneration of the energy surface in a broad region adjacent to the phase boundaries, the occurrence of intermediate O phase, and enhanced piezoelectric properties but with more shallow gradients than those observed in morphotropic solid solutions.

B. Resonance-antiresonance results

The temperature dependence of phase angle θ, relative permittivity $\varepsilon_{33}^T/\varepsilon_0$, piezoelectric coefficient d_{33}, coupling coefficient k_{33}, and mechanical quality factor Q_m for various compositions are provided in Figs. 4(a)–4(e), respectively. The phase transition lines from a previous experimentally determined phase diagram are superimposed for comparison [13].

The θ values [Fig. 4(a)] are normally considered as an indication of degree of poling [49–52]. It is clearly seen that the phase angle shows distinct changes near the phase boundaries, but also, under the same poling conditions, the R and T phases respond quite differently at room temperature to the poling treatment. The room-temperature R phase ($x < 0.40$) shows θ values between 78.9° and 80.1°, which are relatively far from an ideal poled condition of 90°. On the other hand, the room-temperature T phase ($x = 0.60$) is characterized by a much higher θ value of 85.9°. The compositions in the vicinity of the O phase boundary ($x = 0.45$ and 0.50) feature θ values comparable to the ones observed at the T phase, i.e., around 85.5°. Since the phase angle indicates the degree of poling, the variation of the phase angle should reflect the variation of remanent polarization. All compositions present a monotonic decay of θ with increasing temperature that reflects the thermal depolarization of the system. Interestingly, the T phase ($x = 0.60$) presents a much higher poling stability than the R phase. Although the phase angle θ is commonly associated with the degree of poling [49–52], a word of caution is warranted. As depicted in Fig. 4(a), the θ values show local minima around the phase boundaries, more clearly discerned at the R to C phase boundary for $x < 0.40$ (the increase in θ above the Curie temperature T_C for $x = 0.32$ is ∼5°, while for $x = 0.35$ is ∼12°). Naturally, the material cannot repole itself with increasing temperature if no external field is applied. Moreover, these local minima in θ are accompanied by local maxima in d_{33} [Fig. 4(c)]. This contradicts the generally known fact that a higher phase angle is associated with a higher degree
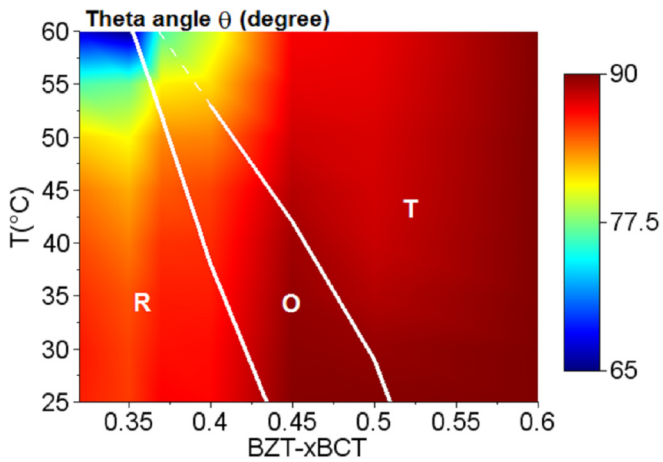
FIG. 5. (Color online) Contour plot of θ angle as a function of temperature and composition. The maximum temperature displayed is 60 °C in order to better visualize the contrast of the poling degree around the phase convergence region. Phase transition lines are superimposed in white [13]. The resolution of the contour plot in the compositional-temperature space is 7 × 8. The variation of properties between the measured points was estimated by linear interpolation between them.

of poling, and thus, higher d_{33} [49–52]. The meaning of this local decrease in θ is believed to be associated with a change in the resistivity of the sample near the phase boundaries. Further experiments are being carried out to determine the physical origins of these observations. A contour plot of θ as function of temperature and composition is shown in Fig. 5. To obtain a better representation of the relation between electromechanical properties and the PPTs, the recent experimentally determined phase boundary lines are also superimposed [13]. In order to emphasize the θ contrast, thus allowing for better visualization, this contour plot is provided up to the temperature of the convergence region ~60 °C. It is clearly observed that, under the same poling conditions, the T phase displays higher θ values than the R phase. More interestingly, in the convergence region the θ values decrease drastically, indicating a much lower degree of poling and thus of net remanent polarization.

The measurements of relative permittivity $\varepsilon_{33}^{T}/\varepsilon_0$ as a function of temperature are displayed in Fig. 4(b). Phase transitions can be derived from this measurement as local maxima [53]. This result is in good agreement with the pseudobinary phase diagram obtained at a different frequency range [13,30] and with the calculated phase diagram obtained in this study (Fig. 1). The maximum values of $\varepsilon_{33}^{T}/\varepsilon_0 \sim 20\,000$ at the R phase are consistent with literature values [12,13].

The piezoelectric coefficient d_{33} as a function of temperature is depicted in Fig. 4(c). The temperature profiles of d_{33} obtained from resonance-antiresonance measurements are in good agreement with a previous study [13]. However, the values of d_{33} are slightly lower which is attributed to the different measuring technique and conditions utilized. The highest d_{33} values for compositions $x < 0.40$ are observed at the Curie line, whereas in the range $0.40 < x < 0.50$, the d_{33} value peaks at the O to T phase boundary. Moreover, for all compositions, residual d_{33} values remain to temperatures even 10 °C above T_C [13,54–56]. Figure 6 presents a contour
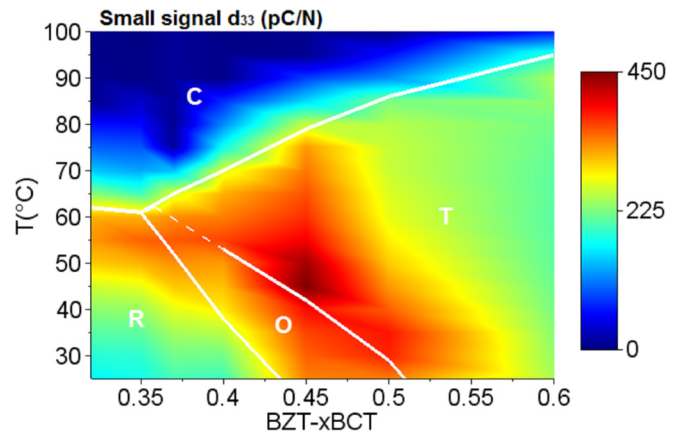

FIG. 6. (Color online) Contour plot of small signal piezoelectric coefficient d_{33} as a function of temperature and composition. Phase transition lines are superimposed in white [13]. The resolution of the contour plot in the composition-temperature space is 7 × 15. The variation of properties between the measured points was estimated by linear interpolation between them.

plot of d_{33} as a function of temperature and composition. The largest d_{33} values occur along the O to T phase boundary with $d_{33} \sim 450$ pC/N, which is in agreement with previous reports [13,30]. Only local maximum values of d_{33} are found in the convergence region and at the R to O phase boundary, which are ~30% below the values at the O to T phase boundary. Moreover, a quasicontinuous d_{33} contrast emerges from the O to T phase boundary, continuing up to the convergence region but with a higher degree of tilting than depicted by phase boundaries. This seems to indicate that more tilted phase boundaries around the convergence region could be expected, which is consistent with recent literature results [57]. Resolving more clearly phase boundaries in such a narrow temperature and compositional ranges requires a more precise technique and it is beyond the scope of the present work.

The coupling coefficient k_{33} is presented in Fig. 4(d). At room temperature, k_{33} values range between 0.4 and 0.6. The highest k_{33} values 0.6 are observed at compositions $x = 0.45$ and 0.50, corresponding to the O phase. In contrast, values around 0.4 and 0.5 are observed for compositions $x < 0.45$ and $x = 0.60$, corresponding to R and T phases, respectively. Comparable and exceptionally large k_{33} values at the O phase were also reported in the literature [35,58]. Although the temperature dependence of k_{33} also shows a relation to the phase boundaries, it does not exhibit variations as pronounced as those observed in d_{33}. In general, it is observed that phase boundaries are accompanied by changes in the slope of k_{33} (i.e., clear local maxima are not observed). Consistent with d_{33}, residual k_{33} values are observed even 10 °C above T_C. A contour plot of k_{33} as a function of temperature and composition is depicted in Fig. 7. It is clearly seen that the T phase features higher values than the R phase. Moreover, a broad maximum in the O phase near room temperature and at the O to T phase boundary is observed. Consistent with the data for d_{33}, the value of k_{33} does not peak in the convergence region.

The mechanical quality factor Q_m is presented in Fig. 4(e). At room temperature, it is observed that increasing the xBCT content leads to a monotonic increase of Q_m values ranging
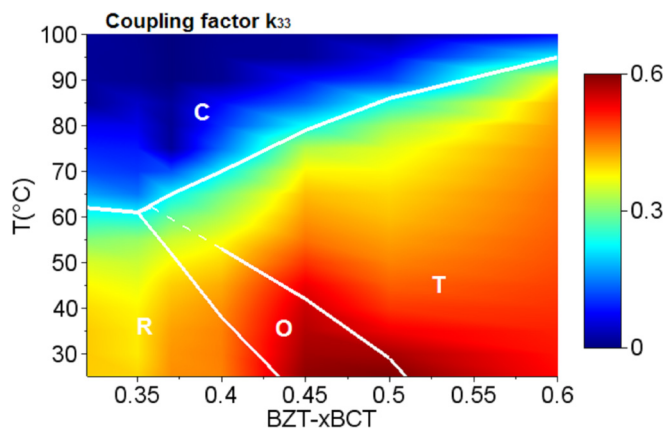
FIG. 7. (Color online) Contour plot of coupling factor k_{33} as a function of temperature and composition. Phase transition lines are superimposed in white [13]. The resolution of the contour plot in the composition-temperature space is 7×15. The variation of properties between the measured points was estimated by linear interpolation between them.

100–160. The highest Q_m values are observed at the T phase ($x = 0.60$). Moreover, Q_m exhibits two different temperature dependencies over the range of composition studied. The composition range with $x < 0.45$ provides a weak linear temperature decrease with average values around 100 at room temperature. With increasing xBCT content, the Q_m profile changes. This results in an increase of Q_m with increasing temperature, indicating a drastic change in the hardening properties when approaching the T phase. Hardening of electromechanical properties with increasing temperature was already observed in the piezoelectric material $(Sr,Ca)_2NaNb_5O_{15}$ [11]. The increase of Q_m with temperature and the almost temperature-independent d_{33} [Fig. 4(c)] make the T phase of BZT-xBCT highly attractive for high power applications.

The temperature dependence of short (s_{33}^E) and open circuit (s_{33}^D) elastic compliances and frequency constant N_{33} are displayed in Figs. 8(a) and 8(b), respectively. Again, the phase boundary lines from a previous phase diagram are superimposed for comparison [13]. The relationship between s_{33}^E and s_{33}^D depends on k_{33} and is given by $s_{33}^E = s_{33}^D/(1 - k_{33}^2)$. Thus both these elastic compliances exhibit local maxima values at phase boundaries [Fig. 8(a)] [44]. For all compositions the differences between s_{33}^E and s_{33}^D smear out quite considerably

at T_C, which indicates thermally induced depoling of the sample. Nevertheless, the values of s_{33}^E and s_{33}^D remain different even several degrees above T_C. This is due to the already described residual k_{33}. Similarly, as observed with the relative permittivity $\varepsilon_{33}^T/\varepsilon_0$, the maximum s_{33}^E values are found in the R phase near the convergence region ($x = 0.35$) with $s_{33}^E = 14 \times 10^{-12} \, m^2/N$. Maximum values computed at the O to T phase boundary ($x = 0.40$) are also quite high and comparable to those obtained in the convergence region, namely $s_{33}^E = 13.8 \times 10^{-12} \, m^2/N$. Cordero *et al.* [36] reported values of $s_{33}^E \sim 14.5 \times 10^{-12} \, m^2/N$, which are consistent with the values reported here. Xue *et al.* [35] reported the temperature-dependent s_{33}^E of BZT-0.5BCT. In their report they observed an $s_{33}^E \sim 19 \times 10^{-12} \, m^2/N$ at the O to T phase boundary, which is higher than that reported here, and might be due to different experimental conditions. The temperature increase of s_{33}^E in the R phase indicates a softening behavior, as also obtained previously by different experimental techniques [36,54]. In the compositions between $x = 0.37$ and $x = 0.50$, s_{33}^E peaks at the O to T phase boundary. With further temperature increase towards T_C, s_{33}^E decreases, which indicates hardening. The T composition with $x = 0.60$ displays a weak temperature dependence of s_{33}^E and relatively low values, which are typical properties of hard materials [59]. Figure 9 shows a contour plot of s_{33}^E as a function of temperature and composition. The O to T phase boundary and the convergence region feature the largest s_{33}^E values. Therefore, the system is mechanically softer in these regions of the phase diagram. The high values of s_{33}^E seem to follow the phase boundaries in a rather broad manner, consistent with the previously reported broad switching dynamics minimum and k_{33} (Fig. 7) [60].

The behavior of the frequency constant N_{33} is summarized in Fig. 8(b). At room temperature, N_{33} values range $\sim$2200–2400 m/s. These values are high, indicating that the BZT-xBCT can vibrate at high resonance frequencies [61]. The temperature dependence shows local minima that clearly reflect the phase transitions. Compositions with $x = 0.32$ and 0.35 reveal a broad minimum in the vicinity of the convergence region, which might indicate the presence of two phase boundaries in a narrow temperature range. It is observed that the R and O phases have N_{33} values that clearly decrease with increasing temperature. In the temperature range where the T phase is stable in compositions with $x > 0.40$, it is found that N_{33} is almost temperature insensitive. Considering that the
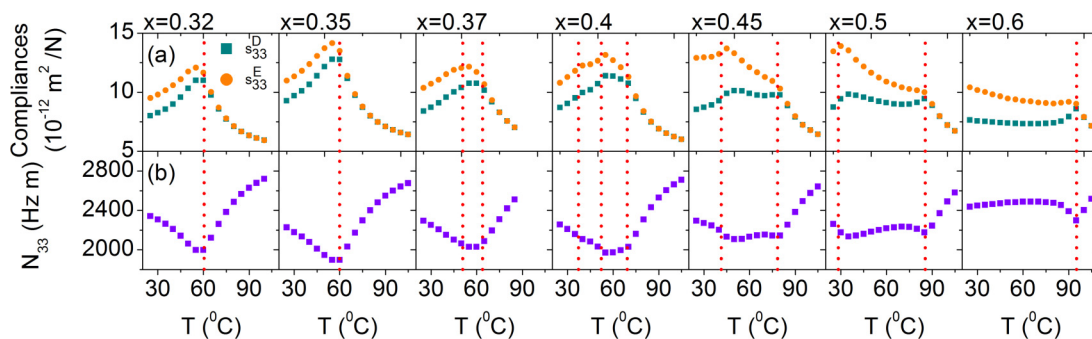

FIG. 8. (Color online) Elastic properties as function of temperature for compositions from $x = 0.32$ to 0.6. (a) Elastic compliances s_{33}^E and s_{33}^D, (b) frequency constant N_{33}. Dotted lines indicate phase transitions [13].
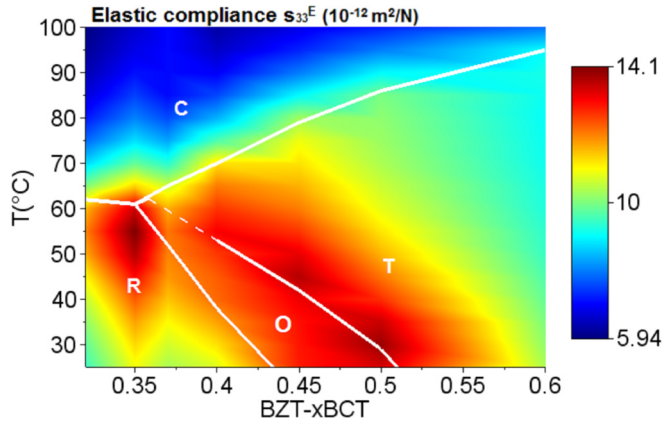
FIG. 9. (Color online) Contour plot of elastic compliance s_{33}^E as a function of temperature and composition. Phase transition lines are superimposed in white [13]. The resolution of the contour plot in the composition-temperature space is 7×15. The variation of properties between the measured points was estimated by linear interpolation between them.

composition with $x = 0.60$ features a wide temperature range in which the T phase is stable with high N_{33} values, as well as the discussed hardening effect given by Q_{m} [Fig. 4(e)], the BZT-xBCT system displays properties suitable for high power applications.

IV. DISCUSSION

As expected, it is clearly observed from both the calculations and the experiments reported here that the anisotropy energy is reduced and the functional properties of BZT-xBCT are maximized in the region near phase boundaries. However, it has been shown that the convergence region and phase boundaries have differing influences on piezoelectric properties, despite the fact that the anisotropy energy is strongly reduced in both regions of the phase diagram. Hence, in contrast to previous suggestions [12] and as recently highlighted [13,30], the piezoelectric activity of BZT-xBCT cannot be fully reconciled solely by a reduction in the anisotropy energy near the phase boundaries.

It was observed that the remanent polarization, as obtained from the phase angle (Fig. 5), varied considerably from 78.9° in the R phase ($x = 0.32$) to 85.9° in the T phase ($x = 0.60$). Therefore, a higher degree of poling is retained in the T phase under equal poling conditions. Since the poling field strength chosen was more than one order of magnitude higher than the coercive field of the specimens studied, unsaturated behavior cannot explain this result. It is suggested that the higher spontaneous polarization (Fig. 1) and deeper energy profiles (Fig. 2) in the T phase explain the observed results. The higher temperature retention of the remanent polarization in the T phase as given by θ [Fig. 4(a)] supports this contention. Moreover, due to a broad area of reduced anisotropy energy, the remanent polarization is most dramatically reduced around PPTs and convergence region, as observed in Fig. 5.

Since a reduction in anisotropy energy is encountered both at the phase boundaries and in the convergence region, more precisely in a broad Y-shaped area (Fig. 3) encompassing the

PPTs, maximized piezoelectric properties should be encountered in this broad region. Nevertheless, as seen in Fig. 6, the highest d_{33} values occurred at the O to T phase boundary. Specifically, the piezoelectric activity at the O to T boundary is 30% higher than in the convergence region. The elastic compliance s_{33}^E values are quite comparable and display maximum values in the convergence region and at the O to T phase boundary. Therefore, elastic softening alone cannot explain the different activity between the convergence region and the O to T phase boundary. Neglecting extrinsic contributions, the small signal d_{33} is proportional to the spontaneous polarization P_3 and relative permittivity, $d_{33} \propto P_3 \cdot \varepsilon_{33}^T/\varepsilon_0$ [62]. Since $\varepsilon_{33}^T/\varepsilon_0$ is maximized around the convergence region, the only reasonable explanation for the observed piezoelectric activity is the reduction of P_3 in this area of the phase diagram. The predicted spontaneous polarization (Fig. 1) indeed indicates that a considerable decay is expected in the convergence region. Moreover, the experimentally obtained remanent polarization indicated by the phase angle θ (Fig. 5) also reveals a decay in the vicinity of the convergence region [$x = 0.32$ in Fig. 5(a)]. The decay of the poled state should result in a reduction in piezoelectric activity in the convergence region. Therefore, both the predictions of the phenomenological theory and the experimental measurements explain the lower d_{33} and k_{33} values in the convergence region. The reduced anisotropy energy leads to greater thermal instability at higher temperatures and is responsible for the decreased spontaneous and remanent polarization values, which results in the diminished piezoelectric activity. These observations indicate that, contrary to previous assumptions [12], reduced anisotropy energy is necessary [46] for enhanced properties but not sufficient for maximized piezoelectric activity. In other words, considering that elastic properties are comparable both in the convergence region and at the O to T phase boundary, maximized piezoelectric activity occurred at the O to T phase boundary due to a higher retained spontaneous/remanent polarization.

If both PPTs are viewed solely from the perspective of reduced anisotropy energy, it is expected that maximum piezoelectric values occur around both phase boundaries and in the interleaving O phase field (Fig. 3). In particular, divergence of the piezoelectric activity should occur along the line where the anisotropy energy vanishes (Fig. 3). Nevertheless, it is found experimentally that near the O to T phase boundary d_{33} values are found to be ~30% higher compared with those at the R to O phase boundary. The different d_{33} values of the two PPTs cannot be explained in terms of spontaneous (Fig. 1) or remanent (Fig. 5) polarization, since they exhibit similar values. In order to discuss this feature of the BZT-xBCT system, it can be alternatively considered that $d_{33} \propto k_{33} \cdot (\varepsilon_{33}^T/\varepsilon_0) \cdot s_{33}^E$ [44]. The measured polycrystalline $\varepsilon_{33}^T/\varepsilon_0$ values are quite comparable at both PPTs at a given temperature [Fig. 4(b)], so they will not be considered for the purposes of this discussion, and thus $d_{33} \propto k_{33} \cdot s_{33}^E$. A broad maximum of k_{33} values is encountered at the O phase. This broad maximum does not favor different piezoelectric activity at the two different PPTs. Moreover, this behavior seems to follow the broad minimum of switching dynamics of the system [60]. This indicates that switching may play a significant role in controlling this property even at subcoercive fields,

as recently suggested by Gao *et al.* [57]. Enhanced switching in this compositional range was also recently confirmed by diffraction studies [63]. Neglecting extrinsic contributions, the only parameter remaining that can potentially explain the different d_{33} values for the two PPTs is s_{33}^{E}. Figure 9 clearly depicts higher s_{33}^{E} values at the O to T phase boundary than at the R to O phase boundary. Therefore, the softening of the system in the vicinity of the O to T phase boundary, at similar values of spontaneous and remanent polarization, explains the enhancement of the piezoelectric activity along this boundary.

Recently Zhang *et al.* [30] performed storage modulus and internal friction measurements on the BZT-0.5BCT as a function of temperature [30]. They observed softening when crossing through the O to T phase boundary, although this softening was not proved as being a general attribute of the whole phase boundary. This softening was also shown by Damjanovic *et al.* [54] from similar measurements. Very recent work by Cordero *et al.* [36] has investigated elastic properties by flexural resonance, dynamic mechanical analysis, and resonance-antiresonance measurements made near the phase boundaries as a function of temperature. It was clearly demonstrated that the elastic softening in the vicinity of the O to T phase boundary is more pronounced than that at the R to O phase boundary, or in the O single phase region. Wang *et al.* [64] also recently demonstrated in a similar BT-based system that enhanced properties occurred along the O to T phase boundary. In fact, this general feature of BT-based piezoceramics was first predicted by the Devonshire phenomenological theory for monodomain single crystals of BT [40]. Devonshire showed that the shear components of the elastic compliance ($s_{44}^{\mathrm{E}} = s_{55}^{\mathrm{E}} = s_{66}^{\mathrm{E}}$) diverge at the O to T phase boundary. This was rationalized by the enhanced shear occurring in the yz or xz planes due to the transition from the T to the O phase with a stepper rise than at the O to R phase boundary. In other words, as the spontaneous polarization of the crystal reorients between [100] and [110] directions, shear components should increase. Moreover, it has to be pointed out that the elastic compliance shear components are proportional to the susceptibility and spontaneous polarization given by $(\eta_{11} + \eta_{12}) \cdot P_{\mathrm{s}}$ [40], which indicates that the maximized properties are associated with a high P_{s}, as previously discussed. Although enhanced shear softening was predicted for monodomain single crystals, it has also been shown experimentally. In the case of BZT-0.5BCT, Xue *et al.* [35] demonstrated that at the O to T phase boundary $s_{44}^{\mathrm{E}} = 37.6 \times 10^{-12}$ m^2/N, which is quite comparable to soft PZT, and almost double that in BT. This result is to be expected considering that the monodomain properties will be reflected in polycrystalline averages as obtained, for example, using the Voigt-Reuss-Hill method [65]. Therefore, the fundamental reason why we experimentally observed higher values of s_{33} along the O to T phase boundary in BT-based ceramics is due to enhanced shear components of elastic compliances [40,46,66].

Although the findings of this work are mostly relevant for BT-based ceramics, an analogy to PZT can be made. Singh *et al.* [67] found that the highest small signal d_{33} does not occur in the M phase bridging the R and T phases. Rather the piezoelectric activity is highest in the T phase on approaching the T to M phase boundary. Consistent with the results reported here, the line of vanishing anisotropy energy in PZT does not coincide with the phase boundary lines [31]. Instead, Singh

et al. [67] attributed this behavior to an anomalous softening reflected by an increased s_{11}^{E}. It can, therefore, be suggested that an analogy may exist when the spontaneous polarization vector shifts through shear from the [100] direction to another direction corresponding to the M (pseudo-orthorhombic) phase. In fact, Sabat *et al.* [59] showed that s_{55}^{E} is more than two times higher than all other elastic compliance components around room temperature near the T to M phase boundary. Cordero *et al.* [36] also highlighted the importance of shear constants in attaining high electromechanical response in both the BZT-xBCT and PZT systems.

This line of reasoning leads to a possible generalization: the different responses of the shear components of the elastic compliance across differing types of phase boundary lines are important considerations in the attainment of maximized electromechanical response. If a change in composition and/or temperature leads to a transition from a T phase to a lower symmetry phase (such as O or M), an increase of shear constants is expected that is much more pronounced that at the transitions from the R phase to one of these lower symmetry phases. Ishibashi and Iwata [66] indeed predicted this increase in the shear components of elastic compliance at the O to T phase boundary. As shown here and elsewhere [31,66], the O to T phase boundary line is not in general coincident with the line along which the anisotropy energy vanishes, or is at least drastically reduced. Hence, the two phenomena are not necessarily direclty related [46].

The design of piezoelectric solid solutions should be pursued considering the interdependent relationships between anisotropy energy, elasticity, and spontaneous/remanent polarization, which will delimit the final achievable piezoelectric activity if extrinsic contributions to the piezoelectric effect are neglected. Maximization of piezoelectric properties will be attained at phase boundaries that present reduced anisotropy energy, high softening, and high spontaneous/remanent polarization. Neither the reduced anisotropy energy, nor elasticity, nor high spontaneous/remanent polarization alone can be considered as sufficient conditions to attain maximized piezoelectric properties. Cordero *et al.* [36] also pointed out that reduced anisotropy energy should only be considered as a necessary, but not sufficient condition, for optimized electromechanical properties. Therefore, in a system with several types of phase transitions (such as BT, BZT-xBCT, or PZT) it is expected that maximized properties occur at the phase boundary that provides the greatest elastic softening, provided that similar levels of reduced anisotropy energy and spontaneous/remanent polarization are maintained.

V. CONCLUSIONS

Experimental properties including phase angle, relative permittivity, piezoelectric and coupling coefficients, and elastic compliance were utilized to establish the relation of the phase diagram with the piezoelectric activity and elastic properties of BZT-xBCT. The predictions of a phenomenological theory for the BZT-xBCT phase diagram were found to be in good qualitative agreement with experiments. Piezoelectric d_{33} values along the orthorhombic to tetragonal phase boundary were found to be 30% higher than those both along the rhombohedral to orthorhombic phase boundary and in the

phase convergence region. The results of this study clearly demonstrate that trade-offs exist between reduced anisotropy energy, retention of spontaneous/remnant polarization, and elastic softening in controlling the piezoelectric activity of the BZT-xBCT system. The largest values of d_{33} are observed along the tetragonal to orthorhombic phase boundary because of a high remanent and spontaneous polarization existing in combination with enhanced shear elastic softening. Based on the combined computational and experimental results the following can be further concluded: (1) In systems with weak first-order phase transitions, strong retention of remanent polarization will occur far from phase boundaries due to increased anisotropy energy. (2) A reduction in anisotropy energy accompanied by elastic softening is a necessary condition for enhanced piezoelectric properties. Since elastic compliance is proportional to the spontaneous polarization, properties can be further maximized where the spontaneous/remanent polarization can be retained. (3) A drastic reduction in anisotropy energy in the absence of enhanced elastic softening will not result in maximized properties.

From an application point of view, a hardening effect in the T phase of BZT-xBCT with increasing temperature is observed and is accompanied by an increased mechanical quality factor. In this compositional range, the BZT-xBCT system is attractive for high power applications.

[1] J. Rödel, W. Jo, K. T. P. Seifert, E. M. Anton, T. Granzow, and D. Damjanovic, J. Am. Ceram. Soc. **92**, 1153 (2009).

[2] Off. J. Eur. Union L **37**, 19 (2003).

[3] Off. J. Eur. Union L **174**, 88 (2011).

[4] J. Rödel, K. G. Webber, R. Dittmer, W. Jo, M. Kimura, and D. Damjanovic, J. Eur. Ceram. Soc. **35**, 1659 (2015).

[5] T. Karaki, T. Katayama, K. Yoshida, S. Maruyama, and M. Adachi, Jpn. J. Appl. Phys. **52**, 09KD11 (2013).

[6] K. Wang, F. Z. Yao, W. Jo, D. Gobeljic, V. V. Shvartsman, D. C. Lupascu, J. F. Li, and J. Rödel, Adv. Funct. Mater. **23**, 4079 (2013).

[7] K. Kobayashi, Y. Doshida, Y. Mizuno, and C. A. Randall, Jpn. J. Appl. Phys. **52**, 09KD07 (2013).

[8] C. A. Randall, A. Kelnberger, G. Y. Yang, R. E. Eitel, and T. R. Shrout, J. Electroceram. **14**, 177 (2005).

[9] T. Tou, Y. Hamaguti, Y. Maida, H. Yamamori, K. Takahashi, and Y. Terashima, Jpn. J. Appl. Phys. **48**, 07GM03 (2009).

[10] Y. Doshida, S. Kishimoto, K. Ishii, H. Kishi, H. Tamura, Y. Tomikawa, and S. Hirose, Jpn. J. Appl. Phys. **46**, 4921 (2007).

[11] Y. Doshida, H. Shimizu, Y. Mizuno, and H. Tamura, Jpn. J. Appl. Phys. **52**, 07HE01 (2013).

[12] W. Liu and X. Ren, Phys. Rev. Lett. **103**, 257602 (2009).

[13] M. Acosta, N. Novak, W. Jo, and J. Rödel, Acta Mater. **80**, 48 (2014).

[14] D. R. J. Brandt, M. Acosta, J. Koruza, and K. G. Webber, J. Appl. Phys. **115**, 204107 (2014).

[15] X. Yan, K. H. Lam, X. Li, R. Chen, W. Ren, X. Ren, Q. Zhou, and K. K. Shung, IEEE Trans. Ultrason. Ferroelect. Freq. Contr. **60**, 1272 (2013).

[16] M. Ahart, M. Somayazulu, R. E. Cohen, P. Ganesh, P. Dera, H. K. Mao, R. J. Hemley, Y. Ren, P. Liermann, and Z. Wu, Nature (London) **451**, 545 (2008).

[17] I. A. Kornev, L. Bellaiche, P. E. Janolin, B. Dkhil, and E. Suard, Phys. Rev. Lett. **97**, 157601 (2006).

[18] J. Frantti, Y. Fujioka, A. Puretzky, Y. Xie, Z. G. Ye, and A. M. Glazer, J. Appl. Phys. **113**, 174104 (2013).

[19] D. Pandey, A. K. Singh, and S. Baik, Acta Crystallogr., Sect. A **64**, 192 (2007).

[20] W. F. Rao and Y. U. Wang, Appl. Phys. Lett. **91**, 052901 (2007).

[21] W. F. Rao and Y. U. Wang, Appl. Phys. Lett. **92**, 102905 (2008).

[22] J. Frantti, Y. Fujioka, and R. M. Nieminen, J. Phys.: Condens. Matter **20**, 472203 (2008).

[23] J. Ouyang and A. L. Roytburd, Acta Mater. **54**, 5565 (2006).

[24] A. Bell, J. Mater. Sci. **41**, 13 (2006).

[25] D. Damjanovic, IEEE Trans. Ultrason. Ferroelect. Freq. Contr. **56**, 1574 (2009).

[26] L. Benguigui, Solid State Commun. **11**, 825 (1972).

[27] G. A. Rossetti, Jr. and A. G. Khachaturyan, Appl. Phys. Lett. **91**, 072909 (2007).

[28] V. A. Isupov, Sov. Phys. Solid State **12**, 1084 (1970).

[29] D. S. Keeble, F. Benabdallah, P. A. Thomas, M. Maglione, and J. Kreisel, Appl. Phys. Lett. **102**, 092903 (2013).

[30] L. Zhang, M. Zhang, L. Wang, C. Zhou, Z. Zhang, Y. Yao, L. Zhang, D. Xue, X. Lou, and X. Ren, Appl. Phys. Lett. **105**, 162908 (2014).

[31] A. A. Heitmann and G. A. Rossetti, Jr., J. Am. Ceram. Soc. **97**, 1661 (2014).

[32] M. C. Ehmke, S. N. Ehrlich, J. E. Blendell, and K. J. Bowman, J. Appl. Phys. **111**, 124110 (2012).

[33] A. Bjørnetun Haugen, J. S. Forrester, D. Damjanovic, B. Li, K. J. Bowman, and J. L. Jones, J. Appl. Phys. **113**, 014103 (2013).

[34] J. Gao, L. Zhang, D. Xue, T. Kimoto, M. Song, L. Zhong, and X. Ren, J. Appl. Phys. **115**, 054108 (2014).

[35] D. Xue, Y. Zhou, H. Bao, C. Zhou, J. Gao, and X. Ren, J. Appl. Phys. **109**, 054110 (2011).

[36] F. Cordero, F. Craciun, M. Dinescu, N. Scarisoreanu, C. Galassi, W. Schranz, and V. Soprunyuk, Appl. Phys. Lett. **105**, 232904 (2014).

[37] B. A. Strukov and A. P. Levanyuk, *Ferroelectric Phenomena in Crystals: Physical Foundations*, Vol. 1 (Springer, New York, 1998).

[38] L. D. Landau and E. M. Lifshitz, *Statistical Physics*, Vol. 5 (Pergamon, Oxford, UK, 1958).

[39] A. F. Devonshire, Philos. Mag. **40**, 1040 (1949).

[40] A. F. Devonshire, Philos. Mag. **42**, 1065 (1951).

[41] G. A. Rossetti, Jr., A. G. Khachaturyan, G. Akcay, and Y. Ni, J. Appl. Phys. **103**, 114113 (2008).

[42] K. Carl and K. H. Hardtl, Phys. Status Solidi A **8**, 87 (1971).

[43] L. A. Shuvalov, J. Phys. Soc. Jpn. **28**, 38 (1970).

[44] IEEE Standard on Piezoelectricity, IEEE Ultrason. Ferr. **176**, 1 (1987).

[45] A. A. Heitmann and G. A. Rossetti, Jr., Philos. Mag. **90**, 71 (2010).

[46] Y. Ishibashi, Ferroelectrics **264**, 197 (2001).

[47] A. G. Khachaturyan, Philos. Mag. **90**, 37 (2010).

[48] V. M. Goldschmidt, Naturwissenschaften **14**, 477 (1926).

[49] J. Wu, D. Xiao, W. Wu, Q. Chen, J. Zhu, Z. Yang, and J. Wang, J. Eur. Ceram. Soc. **32**, 891 (2012).

[50] Q. Chen, Z. Peng, H. Liu, D. Xiao, J. Zhu, and J. Zhu, J. Am. Ceram. Soc. **93**, 2788 (2010).

[51] C. Fujioka, R. Aoyagi, H. Takeda, S. Okamura, and T. Shiosaki, J. Eur. Ceram. Soc. **25**, 2723 (2005).

[52] H. Y. Park, I. T. Seo, M. K. Choi, S. Nahm, H. G. Lee, H. W. Kang, and B. H. Choi, J. Appl. Phys. **104**, 034103 (2008).

[53] E. M. Anton, W. Jo, D. Damjanovic, and J. Rödel, J. Appl. Phys. **110**, 094108 (2011).

[54] D. Damjanovic, A. Biancoli, L. Batooli, A. Vahabzadeh, and J. Trodahl, Appl. Phys. Lett. **100**, 192907 (2012).

[55] J. Hao, W. Bai, W. Li, J. Zhai, and C. Randall, J. Am. Ceram. Soc. **95**, 1998 (2012).

[56] S. Su, R. Zuo, S. Lu, Z. Xu, X. Wang, and L. Li, Curr. Appl. Phys. **11**, S120 (2011).

[57] J. Gao, X. Hu, L. Zhang, F. Li, L. Zhang, Y. Wang, Y. Hao, L. Zhong, and X. Ren, Appl. Phys. Lett. **104**, 252909 (2014).

[58] L. F. Zhu, B. P. Zhang, X. K. Zhao, L. Zhao, P. F. Zhou, and J. F. Li, J. Am. Ceram. Soc. **96**, 241 (2013).

[59] R. Georges Sabat, B. K. Mukherjee, W. Ren, and G. Yang, J. Appl. Phys. **101**, 064111 (2007).

[60] S. Zhukov, Y. A. Genenko, M. Acosta, H. Humburg, W. Jo, J. Rödel, and H. von Seggern, Appl. Phys. Lett. **103**, 152904 (2013).

[61] H. Komiya, Y. Naito, T. Takenaka, and K. Sakata, Jpn. J. Appl. Phys. **28**, 114 (1989).

[62] Q. M. Zhang, H. Wang, N. Kim, and L. E. Cross, J. Appl. Phys. **75**, 454 (1994).

[63] G. Tutuncu, B. Li, K. Bowman, and J. L. Jones, J. Appl. Phys. **115**, 144104 (2014).

[64] D. Wang, Z. Jiang, B. Yang, S. Zhang, M. Zhang, F. Guo, W. Cao, and D. Johnson, J. Am. Ceram. Soc. **97**, 3244 (2014).

[65] R. E. Newnham, *Properties of Materials: Anistropy, Symmetry, Structure* (Oxford University Press, London, 2004).

[66] Y. Ishibashi and M. Iwata, Jpn. J. Appl. Phys. **38**, 1454 (1999).

[67] A. K. Singh, S. K. Mishra, Ragini, D. Pandey, S. Yoon, S. Baik, and N. Shin, Appl. Phys. Lett. **92**, 022910 (2008).